Performance improvement of FSO/CDMA systems over dispersive turbulence channel using multi-wavelength PPM signaling

Ngoc T. Dang[1,2,*] **and Anh T. Pham**[2]

[1] *Posts and Telecommunications Institute of Technology, Hanoi city, Vietnam*
[2] *Computer Communication Lab., The University of Aizu, Aizu-Wakamatsu city, Fukushima 965-8580, Japan*
[*] *ngocdt@ptit.edu.vn*

Abstract: Previous studies show that, compared to on-off keying (OOK) signaling, pulse-position modulation (PPM) is favorable in FSO/CDMA systems thanks to its energy efficiency and simple detection. Nevertheless, when the system bit rate increases and the transmission distance is far, the FSO/CDMA systems using PPM signaling critically suffer from the impact of pulse broadening caused by dispersion, especially when the modulation level is high. In this paper, we therefore propose to use multi-wavelength PPM (MWPPM) signaling to overcome the limitation of PPM. To further improve the system performance, avalanche photodiode (APD) is also used. The performance of the proposed system is theoretically analyzed using a realistic model of Gaussian pulse propagation. To model the impact of intensity fluctuation caused by the atmospheric turbulence, the log-normal channel is used. We find that, by using MWPPM, the effects of both intensity fluctuation and pulse broadening are mitigated, the BER is therefore significantly improved. Additionally, we quantitatively show that the system performance is further improved by using APD, especially when the average APD gain is chosen properly.

OCIS codes: (060.2605) Free-space optical communication;(060.4510) Optical communications.

References and links

1. H. A. Willebrand and B. S. Ghuman, "Fiber optics without fiber," IEEE Spectrum **38**, 40–45 (2001).
2. Q. Liu, C. Qiao, G. Mitchell, and S. Stanton, "Optical wireless communication networks for first- and last-mile broadband access [Invited]," J. Opt. Netw. **4**, 807–828 (2005).
3. T. Ohtsuki, "Performance analysis of atmospheric optical PPM CDMA systems," J. Lightwave Technol. **21**, 406–411 (2003).
4. K. Ohba, T. Hirano, T. Miyazawa, and I. Sasase, "A symbol decision scheme to mitigate effects of scintillations and MAIs in optical atmospheric PPM-CDMA systems," in *Proceedings of IEEE GLOBECOM*, (St. Louis, 2005), pp. 1999–2003.
5. M. Jazayerifar and J. A. Salehi, "Atmospheric optical CDMA communication systems via optical orthogonal godes," J. Lightwave Technol. **54**, 1614–1623 (2006).
6. T. Miyazawa and I. Sasase, "BER performance analysis of spectral phase-encoded optical atmospheric PPM-CDMA communication systems," J. Lightwave Technol. **25**, 2992–3000 (2007).

7. A. T. Pham, T. A. Luu, and N. T. Dang, "Performance bound for Turbo-coded 2-D FSO/CDMA systems over atmospheric turbulence channel," IEICE Trans. Fundamentals. **E93-A**, 1745–1337 (2010).
8. A. Stok and E. H. Sargent, "The role of optical CDMA in access networks," IEEE Commun. Mag. **40**, 83–87 (2002).
9. X. Zhu and J. M. Khan, "Free-space optical communication through atmospheric turbulence channels," IEEE Trans. Commun. **50**, 1293–1300 (2002).
10. C. C. Davis and I. Smolyaninov, "The effect of atmospheric turbulence on bit-error-rate in an on-off keyed optical wireless system," in *Proceedings of SPIE Free-Space Laser Commun. Laser Imaging,* (1997), pp. 126–137.
11. C. Y. Young, L. C. Andrews, and A. Ishimaru, "Time-of-arrival fluctuations of a space-time Gaussian pulse in weak optical turbulence: an analytic solution," Appl. Opt **37**, 7655–7660 (1998).
12. H. Hemmati, *Deep space optical communications* (John Wiley and Sons, 2006).
13. S. M. Navidpour, M. Uysal, and M. Kavehrad, "BER performance of free-space optical transmission with spatial diversity," IEEE Trans. Wireless Comm. **6**, 2813–2819 (2007).
14. T. A. Tsiftsis, , H.G. Sandalidis, G. K. Karagiannidis, and M. Uysal, "Optical wireless links with spatial diversity over strong atmospheric turbulence channels," IEEE Trans. Wireless Comm. **8**, 951–957 (2009).
15. E. Bayaki, R. Schober, and R.K. Mallik, "Performance analysis of MIMO free-space optical systems in gamma-gamma fading," IEEE Trans. Comm. **57**, 3415-3424 (2009).
16. I. Djordjevic, W. Ryan, B. Vasic, *Coding for optical channels* (Springer, 2010).
17. G. Agrawal, *Nonlinear fiber optics* (Academic Press, 2006).
18. G. C. Yang and W. C. Kwong, *Prime code with application to CDMA optical and wireless networks* (Artech House, 2002).

1. Introduction

Over past few years, free-space optical communication (FSO) has attracted considerable attention for a variety of applications thanks to its cost-effectiveness, license-free, quick deployment and flexibility [1]. There are recently some efforts to introduce FSO to the first-mile access environment [2]. To support multiple users in access environment, the optical code-division multiple-access (CDMA) systems based on FSO (FSO/CDMA) have been recently proposed and generated much interest [3] - [7]. This is due to the additional advantages of CDMA technique, including asynchronous access, efficient use of resource, scalability and inherent security [8].

A major impairment over FSO links is the atmospheric turbulence, a phenomenon occurs as a result of the variations in the refractive index due to inhomogeneties in temperature and pressure changes [9]. These index inhomogeneities can deteriorate the quality of the received signal and can cause fluctuations in both the intensity and the phase of the received signal. These fluctuations can lead to an increase in the link error probability, which limits the performance of FSO systems [10]. Moreover, propagating pulses may be influenced by pulse broadening owing to turbulence. Two possible causes that exist for this pulse broadening are scattering and pulse wander (dispersion) [11].

To mitigate atmospheric turbulence effects, previous FSO/CDMA studies have often employed M-ary pulse-position modulation (M-PPM) as an energy-efficient transmission [3] - [7]. M-PPM also avoids adaptive threshold adjustment required in on-off keying (OOK). Previous studies, which ignore the pulse broadening effect, show that M-PPM is effective in reducing intensity fluctuation. However, to provide a comprehensive performance analysis of FSO/CDMA systems, the effect of pulse broadening should be evaluated. Moreover, its effect will be considerable and cannot be ignored since FSO systems, and especially FSO/CDMA systems using M-PPM, require to send high chip rate (i.e., short pulse) through turbulence channel.

In this paper, we therefore propose to use a realistic model of Gaussian pulse propagation in order to comprehensively analyze the effects of atmospheric turbulence on the performance of FSO/CDMA systems. This model should be able to analyze all effects of atmospheric turbulence, including intensity fluctuation, pulse broadening, and attenuation. Additionally, numerous noises and interference, including shot noise, background noise, thermal noise and multiple-access interference (MAI), will be included in the analysis.

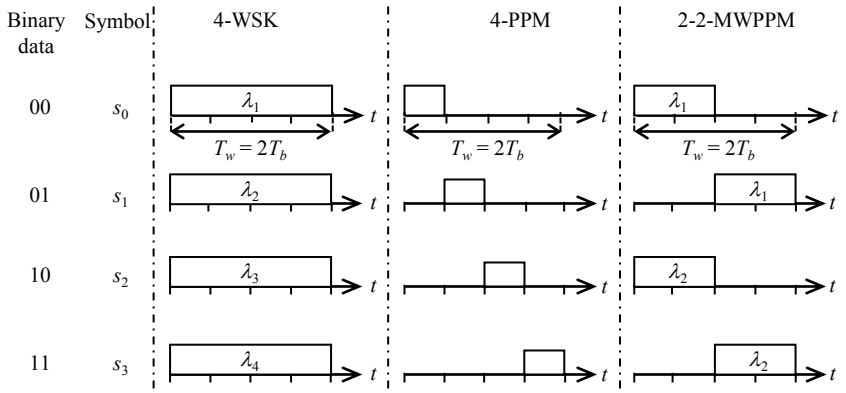

Fig. 1. Modulation schemes: 4-WSK; 4-PPM; and 2-2-MWPPM.

To avoid using short pulse for M-PPM with high-level modulation (i.e., M is large), we propose to use multi-wavelength PPM (MWPPM), which is a combination of wavelength shift keying (WSK) [12] and PPM. Hence, MWPPM is characterized by two parameters, the number of wavelengths (L) and the number of positions (M). In a L-M-MWPPM, an optical pulse representing one of N symbols can be transmitted in one of M time slot at one of L wavelengths as shown in Fig. 1, where $N = L \times M$. As a result, thanks to the use of L wavelengths, the modulation level of M-PPM can be increased L times without increasing the chip rate. In addition, MWPPM avoids the linear increase in required average laser power with data rate that is characteristic of WSK [12]. Finally, avalanche photodiode (APD) is also proposed to be used at the receiver to further improve the system performance.

The rest of the paper is organized as follows. Section 2 presents the model of atmospheric turbulence channel. The principle of MWPPM is introduced in Section 3. The model of FSO/CDMA system using MWPPM and its performance analysis are presented in Section 4 and Section 5, respectively. Section 6 shows the numerical results and discussion. Finally, Section 7 concludes the paper.

2. Atmospheric turbulence channel model

2.1. Log-normal channel model

The atmosphere is not an ideal communication channel. Inhomogeneities in the temperature and pressure of the atmosphere lead to refractive index variations along the transmission path, which is commonly known as atmospheric turbulence. It produces a variety of phenomena such as frequency selective attenuation, absorption, scattering, and scintillation. When an optical beam propagates through the atmosphere, the signal intensity as observed with an optical detector at the end of the path is fluctuated randomly. This is referred to as scintillation, and it is also the major impairment of FSO communication systems.

It is difficult to determine the probability density function (pdf) for the intensity fluctuations under arbitrary atmospheric conditions and beam parameters. However, based on scintillation statistics, various mathematical models have been proposed such as log-normal [13], Gamma [14] or Gamma-Gamma [15] distribution. In this paper, as we consider weak turbulence scenario, the log-normal distribution model is adopted.

A random variable B has a log-normal distribution if the random variable $A = \ln B$ has a

normal (i.e., Gaussian) distribution. Thus, if the amplitude of the random path gain B is I, the optical intensity $I = B^2$ is also lognormally distributed in this case. Consequently, the fading channel coefficient, which models the channel from the transmit aperture to the receive aperture, is given by

$$h = \frac{I}{I_m} = \exp(2X), \tag{1}$$

where, I_m is the signal light intensity, actually at the transmitter, without turbulence; I is the signal light intensity, actually at the receiver, with turbulence. Log-amplitude X, which is the identically distributed normal random variable with mean μ_x and standard deviation σ_x, can be expressed as

$$f_x(X) = \frac{1}{\sqrt{2\pi}\sigma_x} \exp\left(-\frac{(X-\mu_x)^2}{2\sigma_x^2}\right). \tag{2}$$

To ensure that the fading does not attenuate or amplify the average power, we normalize the fading coefficients so that E(h)=1. Doing so requires the choice of $\mu_x = -\sigma_x^2$. Substituting Eq. (1) in Eq. (2), the distribution of light intensity fading induced by turbulence, which is also a log-normal distribution, can be expressed as

$$f_I(h) = \frac{1}{\sqrt{8\pi}h\sigma_x} \exp\left(-\frac{\left[\ln(h) + 2\sigma_x^2\right]^2}{8\sigma_x^2}\right), \tag{3}$$

where σ_x^2, under weak turbulence conditions, are given by [16]

$$\sigma_x^2 = 0.124 \left(\frac{2\pi}{\lambda}\right)^{7/6} z^{11/6} C_n^2, \tag{4}$$

where λ is the wavelength and z is the link distance in meters. C_n^2 stands for the refractive index structure coefficient.

2.2. Pulse propagation model

To obtain explicit expressions concerning the time-domain spreading of a pulse wave propagating through atmospheric turbulence, let us assume that the input waveform is the Gaussian pulse. The amplitude of the Gaussian pulse is described by

$$A_i(t) = \sqrt{P_p} \exp\left(-\frac{t^2}{T_0^2}\right), \tag{5}$$

where P_p and T_0 are the peak power and the half-width (at the $1/e$ point) of the input pulse, respectively.

Considering the losses caused by absorption and scattering of light as well as beam divergence, the amplitude of optical pulse at the receiver located at distance z (km) from the transmitter can be expressed as

$$A_r(t) = \sqrt{P_p \frac{A}{\pi\theta^2 z^2} \exp(-\beta z)} \frac{T_0}{\sqrt{T_0^2 + 8\alpha}} \exp\left(-\frac{t^2}{T_0^2 + 8\alpha}\right), \tag{6}$$

where A is receiver aperture area. θ and β are beam divergence angle in mrad and attenuation coefficient in km^{-1}, respectively. The parameter α is given by [11]

$$\alpha = \frac{0.3908 C_n^2 z L_0^{5/3}}{c^2}, \tag{7}$$

where L_0 is the outer scale of turbulence and c is the light velocity. In Eq. (7), z is the link distance in meters.

3. Multi-wavelength PPM signaling

A *L*-*M*-MWPPM is a combination of *L*-WSK and *M*-PPM, where *L* is the number of transmitted wavelengths and *M* is the modulation level of PPM. In this technique, each block of $b = \log_2 N$ data bits is mapped to one of *N* possible symbols $(s_0, s_1, ..., s_{N-1})$. In each *b*-bit block, the first $\log_2 L$ bits are used for WSK and the remaining $\log_2 M$ ones for PPM, as shown in Fig. 2. The symbol intervals, T_w, are divided into *M* time-disjoint time slots and an optical pulse with constant power is sent in one of these *M* time slots while remaining $M-1$ time slots are empty. Moreover, the optical pulse can take on any of *L* disjoint wavelengths. Therefore, the dimensionality of the signal-space has been increased from *M* dimensions for PPM to $L \times M$ dimensions.

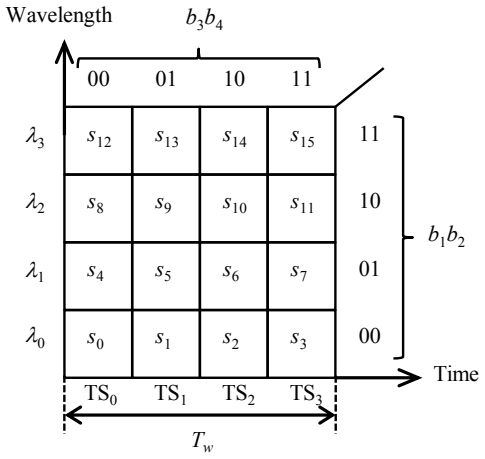

Fig. 2. Principle of 4-4-MWPPM.

Figure 2 shows the principle of 4-4-MWPPM. Each input data of four bits is divided into two parts. The first two bits (b_1b_2) decide the wavelength of the optical pulse while the last two bits (b_3b_4) govern the position (or time slot, TS) that the pulse is transmitted. For example, if the 4-bit input data is 0111, the 4-4-MWPPM modulator will send an optical pulse at time slot 3 of the symbol interval and on wavelength λ_1.

4. FSO/CDMA systems using MWPPM

A FSO/CDMA system using *L*-*M*-MWPPM is shown in Fig. 3. For illustrative purposes, the principle of the FSO/CDMA system using 2-2-MWPPM is explained in detail.

In the transmitter side, each block of $b = \log_2 N$ data bits is first sent to a MWPPM modulator, whose block diagram is illustrated in Fig. 4(a). At the MWPPM modulator, the first $\log_2 L$ bits of the *b*-bit block are detected by a WSK modulator to decide the wavelength of the MWPPM symbol by sending the remaining bits to its corresponding output. The remaining bits are entered into a PPM modulator to govern the position, i.e., time slot, of the transmitted pulse during a symbol interval (T_w). Finally, optical pulse representing for a MWPPM symbol is encoded by an OCDMA encoder, where it is spread into a chip sequence including chip "1" and "0". A chip "1" is an optical pulse while a chip "0" is no pulse. The number of chips in a sequence is equal to the code length (F) of the signature code generated by the code generator. Each chip "1" is assumed as a Gaussian pulse, which will be affected by pulse broadening effect and attenuation during propagation over dispersive turbulence channel.

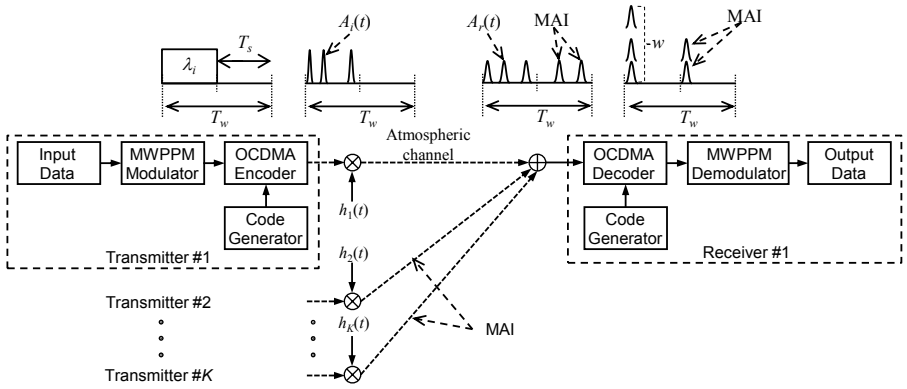

Fig. 3. A FSO/CDMA system using *L*-*M*-MWPPM.

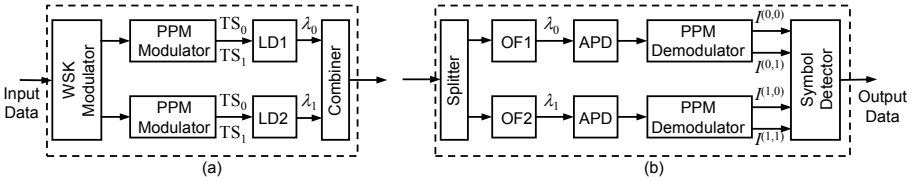

Fig. 4. 2-2-MWPPM modulator/demodulator: (a) modulator and (b) demodulator.

At the receiver, signals from all transmitters are collected and sent to an OCDMA decoder, which is controlled by the code generator. Received signals including not only the signal from desired transmitter but also the signals from interfering transmitters, i.e., MAI, are decoded by the OCDMA decoder. Next, decoded signal goes into a MWPPM demodulator, whose block diagram is shown in Fig. 4(b). Here, the wavelength of the MWPPM symbol is first detected by optical filters (OF). The optical signal is then converted into the electrical one by an APD for PPM demodulating process at a PPM demodulator. Each PPM demodulator has M outputs which contain the electrical currents corresponding the intensity of the received signal at M time slots of a symbol interval. Finally, at symbol detector, integrated photocurrents over $N = L \times M$ inputs corresponding to N symbols, are compared. The input with the highest current determines the transmitted symbol and recovers the binary data.

5. Performance analysis

5.1. Signal and noise

In this subsection, we first determine the parameters of transmitted Gaussian pulse, $A_i(t)$, representing for chip "1" based on system's parameters. For the bit rate of R_b bit per second, the *L*-*M*-MWPPM symbol intervals have a duration of $T_w = \log_2 N/R_b$, and the duration of time slots is written as $T_s = T_w/M$. As F chips is send in each time slot, the chip duration can be expressed as $T_c = T_s/F$. The relation between the half-width of Gaussian pulse (T_0) and its full-width (T_c) can be expressed as [17]

$$T_0 = \frac{\log_2 N/R_b}{MF4\ln 2}. \tag{8}$$

For a fair comparison with other systems, the analysis is considered under a constraint on the average transmitted power per bit denoted as P_s. The relation between P_c and P_s is given by $P_c = M(\log_2 N)P_s/w$. In addition, the peak power of transmitted Gaussian pulse (P_p) can be computed as

$$P_p = \frac{\sqrt{2}T_c}{\sqrt{\pi}T_0}P_c. \tag{9}$$

The derivation of Eq. (9) is presented in detail in the Appendix.

At the receiver, after the OCDMA decoding, the decoded signal includes optical pulses from the desired transmitter and interfering ones (MAI pulses) from remaining transmitters. More specifically, there are w pulses from the desired user, which is equal to the code weight. As well, each interfering user contributes at most γ pulses corresponding to the cross-correlation value between two different codes.

We assume that all users are synchronized, i.e., no time delay among signals (the worst performance). Also, their transmitted power per bit and the distance from all transmitters to the receiver are the same. The optical field output from a filter can be expressed as

$$E^{(u,v)}(t) \propto aw\sqrt{h_d}A_r(t)\exp\left\{j\left(\omega_{\lambda_v}t+\phi_{\lambda_v}\right)\right\} + \sum_{k=1}^{\kappa^{(u,v)}}\sqrt{h_k}A_r(t)\exp\left\{j\left(\omega_{\lambda_v}t+\phi_{\lambda_v}\right)\right\}, \tag{10}$$

where $a = 1$ when the desired transmitter send a symbol at the time slot u on wavelength λ_v ($0 \le u \le M-1$ and $0 \le v \le L-1$), otherwise a is equal to zero. h_d and h_k denote the intensity fluctuation caused by atmospheric turbulence on the desired user and interfering user k. $\kappa^{(u,v)}$ is the total of number of interfering pulses at the time slot u and wavelength λ_v. In addition, ω_{λ_v} and ϕ_{λ_v} are the optical frequency and phase of the optical carrier corresponding to the wavelength λ_v, respectively.

The corresponding current at the output of ADP is derived by square law detection. The mean current on time slot u can be expressed as

$$\mu_{I^{(u,v)}} = \Re\bar{g}\bar{P}_c\left(wh_d + \sum_{k=1}^{\kappa^{(u,v)}}h_k\right), \tag{11}$$

where $\Re$ and $\bar{g}$ are the responsivity and average gain of APD, respectively. $\bar{P}_c$ is the average power per chip considering pulse broadening effect, whose value can be computed as

$$\bar{P}_c = \frac{1}{T_c}\int_{-T_c/2}^{T_c/2}|A_r(t)|^2\,dt. \tag{12}$$

The variance of receiver noise current can be modeled as a zero-mean Gaussian process. It includes shot noise and thermal noise and can be expressed as

$$\sigma^2_{I^{(u,v)}} = 2e\Re F_a\bar{g}^2\left(\bar{P}_c wh_d + \bar{P}_c\sum_{k=1}^{\kappa^{(u,v)}}h_k + P_b\right)\Delta f + \frac{4k_BT}{R_L}\Delta f, \tag{13}$$

where e is the electron charge; k_B is Boltzmann constant; T is the absolute temperature; and R_L is the load resistance. P_b denotes optical background power and $\Delta f = B_e/2$ is the effective noise bandwidth with $B_e = MR_b/\log_2 N$. F_a is the excess noise factor of the APD, which is given by

$$F_a = \zeta\bar{g} + \left(2 - \frac{1}{\bar{g}}\right)(1-\zeta), \tag{14}$$

where ζ denotes the ionization factor.

5.2. *Bit error rate*

In this subsection, we present the method to calculate the bit error rate (BER) of the FSO/CDMA system using *L*-*M*-MWPPM and APD. It is worth noting that *M*-PPM and *L*-WSK are the special cases of *L*-*M*-MWPPM with $L = 1$ and $M = 1$, respectively. Denoting P_e as the symbol error probability, the bit error rate of the system then can be derived as

$$BER = \frac{N}{2(N-1)} P_e. \tag{15}$$

We assume that the transmitted data is large enough so that the probabilities of sending any symbols are the same. Without the loss of generality, we also assume that symbol s_0 is transmitted and there is no pulse interfering to this symbol (upper bound case), by using union bound technique, the upper bound to the instantaneous symbol error probability over a K user channel can be expressed as [7]

$$\begin{aligned} P_e &\leq \sum_{v=1}^{L-1} \sum_{u=1}^{M-1} \Pr\{I^{(0,0)} \leq I^{(u,v)} | s = s_0\} = \\ &= (N-1) \sum_{l_1=0}^{\gamma(K-1)} \Pr\left\{\kappa^{(1,0)} = l_1\right\} \Pr\{I^{(0,0)} \leq I^{(1,0)} | s = s_0, \kappa^{(1,0)} = l_1\} \end{aligned} \tag{16}$$

where s represents the transmitted symbol. $\kappa^{(1,0)}$ is the total number of pulses interfering to symbol s_1. γ is the maximum cross-correlation between two users' signature codes. $I^{(0,0)}$ and $I^{(1,0)}$ are the photocurrent representing symbols s_0 and s_1, respectively.

Interfering pulses are those from interfering users whose position match with a pulse representing a chip "1" of the receiver's signature code. The probability that a pulse exists in a chip duration of a signature code equals w/F. On the other hand, the probability that this pulse will overlap another pulse from an interfering user is again equal to w/F. This result leads to the probability of a single chip interference (overlap) between any two codes at chip duration being equal to w^2/F^2. Hence, $\kappa^{(1,0)}$ can be modeled as a binomial random variable with probability w^2/F^2. As a result, the first term in Eq. (16) can be expressed as

$$\Pr(\kappa^{(1,0)} = l_1) = \binom{\gamma(K-1)}{l_1} \left(\frac{w^2}{F^2}\right)^{l_1} \left(1 - \frac{w^2}{F^2}\right)^{N-1-l_1}. \tag{17}$$

The last term in Eq. (16) is calculated by

$$\Pr(I^{(0,0)} \leq I^{(1,0)} | s = s_0, \kappa^{(1,0)} = l_1) = \int_{\vec{h}} f_I(\vec{h}) \times Q\left(\frac{\mu_{I^{(0,0)}}(\vec{h}) - \mu_{I^{(1,0)}}(\vec{h})}{\sqrt{\sigma^2_{I^{(0,0)}}(\vec{h}) + \sigma^2_{I^{(1,0)}}(\vec{h})}}\right) d\vec{h}, \tag{18}$$

where $Q(.)$ is the Q function. $\mu_{I^{(0,0)}}$, $\sigma^2_{I^{(0,0)}}$, $\mu_{I^{(1,0)}}$, and $\sigma^2_{I^{(1,0)}}$ are the means and variances of $I^{(0,0)}$ and $I^{(1,0)}$, respectively. Based on Eqs. (11) and (13) and under assumption that there are no MAI pulses interfering to symbol s_0, i.e., the worst performance as the impact of MAI on

Table 1. System Parameters and Constants.

Name	Symbol	Value
Boltzmann's constant	k_B	1.38×10^{-23} W/K/Hz
Electron charge	e	1.6×10^{-19} C
Load resistance	R_L	50 Ω
Receiver temperature	T	300 K
PD responsivity	$\Re$	0.5 A/W
Background power	P_b	-40 dBm
Ionization factor	ζ	0.5
Outer scale of turbulence	L_0	10 m
Attenuation coefficient (clear air)	β	0.1 km^{-1}
Beam divergence angle	θ	1 mrad
Receiver aperture diameter	d_R	8 cm
Wavelength	λ	1550 nm
Wavelength interval in MWPPM	$\Delta\lambda$	0.8 nm
Refractive index structure coeff.	C_n^2	10^{-14} $\text{m}^{-2/3}$
Prime number	p_s	37

symbol s_0 is positive, their values can be expressed as

$$\begin{aligned}
\mu_{I(0,0)} &= \Re \bar{g} \bar{P}_c w h_d, \\
\sigma^2_{I(0,0)} &= 2e\Re F_a \bar{g}^2 (\bar{P}_c w h_d + P_b)\Delta f + \frac{4k_B T}{R_L}\Delta f, \\
\mu_{I(1,0)} &= \Re \bar{g} \bar{P}_c \sum_{k=1}^{\kappa_u} h_k, \\
\sigma^2_{I(1,0)} &= 2e\Re F_a \bar{g}^2 \left(\bar{P}_c \sum_{k=1}^{\kappa_1} h_k + P_b \right) \Delta f + \frac{4k_B T}{R_L}\Delta f.
\end{aligned}$$

6. Numerical results

In this section, we investigate the performance of APD-based FSO/CDMA systems using OOK, PPM, WSK, and MWPPM. We use prime code for FSO/CDMA system since it is popular and widely used in optical CDMA system. Each code of a code set constructed from a prime number (p_s) has the code length of $F = p_s^2$, code weight of $w = p_s$, and the cross-correlation between two any codes of $\gamma = 2$ [18]. The system parameters and constants used in the analysis are shown in Table 1.

First, Fig. 5 shows BER of FSO/CDMA systems using OOK, M-PPM, and L-M-MWPPM versus the transmitted power per bit when $z = 1.5$ km, $K = 32$ users, and $R_b = 1$ Gbps. It is seen that the system performance is significantly improved by using either PPM or MWPPM. However, we find that M-PPM with $M > 16$ does not help to reduce system's BER. BER of FSO/CDMA system using 32-PPM is even worse than that of the one using 8-PPM. This is because the system using 32-PPM has higher chip rate and thus pulse broadening effect is dominant compared to intensity fluctuation one.

The limitation of M-PPM can be overcome by using L-M-MWPPM, which has an ability of mitigating both intensity fluctuation and pulse broadening effects, simultaneously. Figure 5

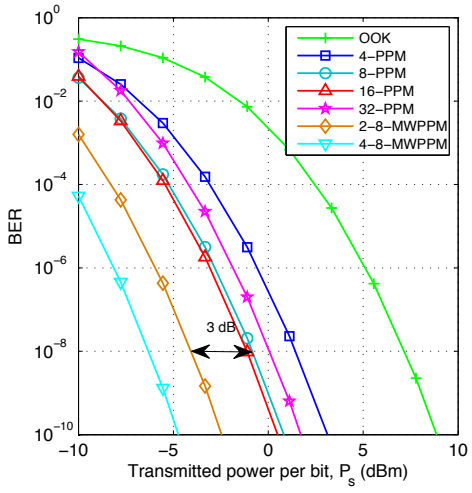

Fig. 5. BER versus the transmitted power per bit with $z = 1.5$ km, $\bar{g} = 30$, $K = 32$ users, and $R_b = 1$ Gbps

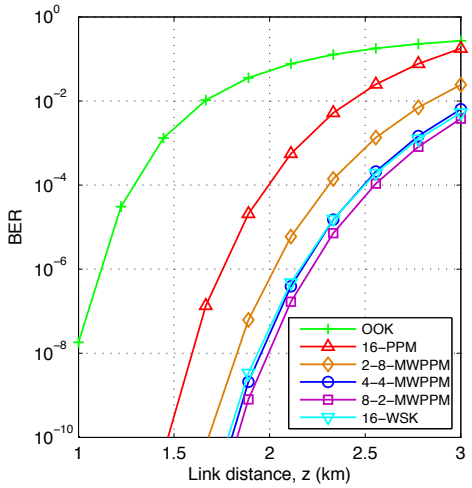

Fig. 6. BER versus the link distance z with $P_s = 0$ dBm, $\bar{g} = 30$, $K = 32$ users, and $R_b = 1$ Gbps

shows that the required transmitted-power per bit to achieve the same BER of the system using 2-8-MWPPM is about 3 dB lower than that of the one using 8-PPM. The power gain of 2-8-MWPPM compared to 8-PPM comes from the fact that 2-8-MWPPM helps to reduce the power loss caused by pulse broadening effect thanks to the increase of the pulse width compared with 8-PPM. Actually, according to Eq. (8), the pulse width of the system using 2-8-MWPPM is equal to 4/3 the pulse width of the one using 8-PPM.

The advantage of MWPPM in reducing the effects of atmospheric turbulence is further highlighted in Fig. 6. In this figure, we fix $P_s = 0$ dBm and investigate the BER versus the link

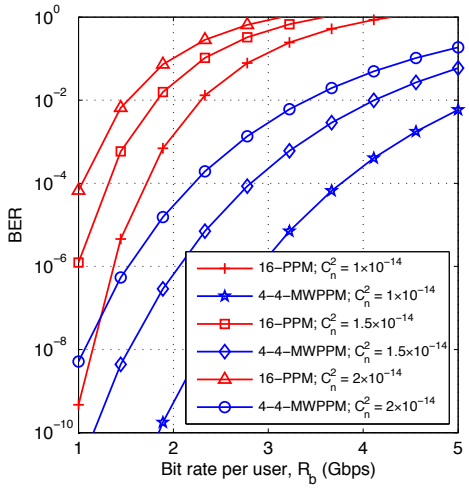

Fig. 7. BER versus the bit rate per user with $P_s = 0$ dBm, $\bar{g} = 30$, $z = 1.5$ km, and $K = 32$ users.

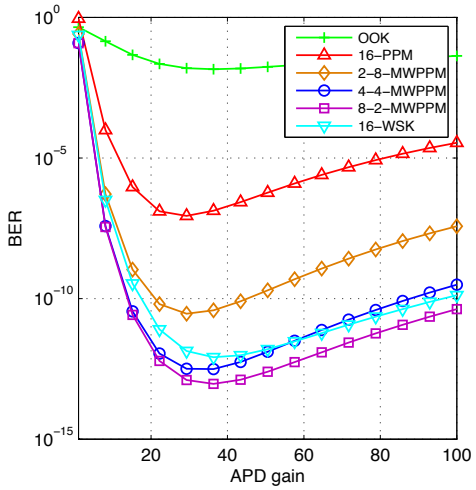

Fig. 8. BER versus the average APD gain ($\bar{g}$) with $P_s = -2$ dBm, $z = 1.5$ km, $K = 32$ users, and $R_b = 1$ Gbps.

distance for OOK, PPM, WSK, and MWPPM systems. The number of simultaneous users and the user bit rate are kept the same as in Fig. 5 while the modulation level is fixed to 16. Thanks to the reduction of pulse broadening effect, the link distance in the FSO/CDMA system using MWPPM can be extended in comparison to the one using OOK or PPM. For example, the maximum link distance in the 8-2-MWPPM system is 0.4 km longer than that of the 16-PPM system. Also, 8-2-MWPPM overcomes 16-WSK (i.e., 16-1-MWPPM) in terms of maximum link distance since WSK, although can also reduce the pulse broadening effect, requires more transmitted power per bit than that of MWPPM.

Next, in Fig. 7, BER is investigated versus the bit rate per user with $z = 1.5$ km, $K = 32$ users,

and $P_s = 0$ dBm. We can observe that the increase of atmospheric turbulence effects (i.e., C_n^2) causes the reduction of the bit rate per user. Also, the FSO/CDMA system using L-M-MWPPM can support higher bit rate per user compared to the one using M-PPM. More specifically, when $C_n^2 = 10^{-14}$, the user bit rate that FSO/CDMA system using 16-PPM can supported (at BER of 10^{-6}) is about 1.35 Gbps. By using 4-4-MWPPM, more than double bit rate per user (i.e., 3.0 Gbps) can be achieved. When $C_n^2 = 2 \times 10^{-14}$, the bit rate per user (at BER of 10^{-6}) of the system using 16-PPM drops below 1 Gbps while it is 1.5 Gbps for the one using 4-4-MWPPM.

Finally, Fig. 8 shows BER versus the average APD gain with $P_s = -2$ dBm. It is seen that BER of FSO/CDMA systems with APD receiver are significantly reduced in comparison with the ones without APD receiver (i.e., $\bar{g} = 1$). The optimum average APD gain, at which BER is smallest, is around 30. When APD gain is larger than 30, APD shot noise becomes considerable thus the system performance is degraded, i.e., BER increases.

7. Conclusion

We have presented a comprehensive study of the effects of atmospheric turbulence, including intensity fluctuation and pulse broadening, on the performance of FSO/CDMA systems using OOK, PPM, WSK, and MWPPM. A realistic model of Gaussian pulse propagation is used for analyzing the BER. The numerical results show that M-PPM with $M > 16$ should not be used as it requires to send short pulse, which is more affected by pulse broadening effect. By using MWPPM, the effect of both intensity fluctuation and pulse broadening can be mitigated thus the system's BER is reduced. In addition, we found that the system performance is significantly improved by using APD, especially when the average APD gain is chosen properly.

Appendix

The average power of transmitted Gaussian pulse, P_c, is defined as

$$P_c = \frac{1}{T_c} \int_{-T_c/2}^{T_c/2} |A_i(t)|^2 dt. \tag{19}$$

We assume that the amplitude of transmitted Gaussian pulse is decreased so that the borders of the chip duration, $-T_c/2$ and $T_c/2$, can be replaced by $-\infty$ and ∞ as integration limits. Equation (19) can be written as

$$\begin{aligned} P_c &= \frac{P_p}{T_s} \int_{-\infty}^{\infty} \exp(-\frac{2t^2}{T_0^2}) dt \\ &= P_p \frac{T_0}{\sqrt{2}T_c} \int_{-\infty}^{\infty} \exp(-x^2) dx = P_p \frac{\sqrt{\pi} T_0}{\sqrt{2} T_c}, \end{aligned} \tag{20}$$

where $x = \sqrt{2}t/T_0$ and the Gaussian integral $\int_{-\infty}^{\infty} \exp(-x^2) dx$ is equal to $\sqrt{\pi}$. From Eq. (20), Eq. (9) can be derived.

Acknowledgment

The authors would like to thank the reviewers for their through reviews and useful suggestions for improving the readability of this paper.